Supplementary Information (SI) for Green Chemistry.

Supporting Information

Oxygen-harvesting carbon dot photocatalysts for ambient tandem oxidative synthesis of quinazolin-4(*3H*)-ones

Bidyutjyoti Dutta,[a,b] Bramhaiah Kommula,[b,c] Kiran Kanwar,[b] Ankur K. Guha,[d] Ujjal K. Gautam,[b*] Diganta Sarma[a*]

[a] *Department of Chemistry, Dibrugarh University, Dibrugarh-786004, Assam, India*
[b] *Department of Chemical Sciences, Indian Institute of Science Education and Research Mohali, Manauli-140306, Punjab, India*
[c] *Department of Chemistry, St. Joseph's University, Bengaluru-560027, Karnataka, India*
[d] *Department of Chemistry, Cotton University, Guwahati-781001, Assam, India*
Corresponding author Email:dsarma22@dibru.ac.in, ujjalgautam@iisermohali.ac.in

TABLE OF CONTENTS

1) General information

All reactions were carried out in the oven dried glassware under atmospheric conditions unless otherwise noted. Starting materials and solvents were obtained from common commercial sources and used without further purification. All reported yields are isolated yields. TLC was carried out using aluminium sheets pre-coated with silica gel $60F_{254}$ (Merck) and was visualized under 254 nm UV light. ^1H NMR (400 & 500 MHz) and ^{13}C NMR (100 & 125 MHz) were recorded on a Bruker Avance 400 MHz spectrometer using TMS as an internal standard. Chemical shifts are reported in parts per million (ppm), downfield from residual solvents peaks and coupling constants are reported as Hertz (Hz). Splitting patterns are designated as s (singlet), d (doublet), t (triplet), q (quartet), dd (doublet of doublet), br(broad) and m (multiplet, for unresolved lines). The mass spectra were recorded on a Q-TOF micromass (YA-105) spectrometer in ESI (electrospray ionization) mode. X-ray diffractograms (XRD) were recorded on a Rigaku Ultima IV diffractometer with Cu Kα radiation (10-80° range). UV-visible absorption and steady-state photoluminescence (PL) measurements were carried out using PerkinElmer, UV/VIS Lamba 365, and Horiba Scientific instruments, respectively. The quantum yield (QY) of the as-synthesized CDs was calculated by taking a quinine sulfate as the reference (QY ~54 %) in 0.1 M H_2SO_4. Time-correlated single photon counts (TCSPC) measurements were recorded using a TCSPC, Fluorocube, Horiba Jobin Yvon, NJ. For the measurements, a ~375 nm laser diode (NanoLED, Horiba Scientific) was used as an excitation source and, lifetimes of as-synthesized CDs were recorded at various emission wavelengths (400-600 nm). Fourier-transformed infrared spectroscopy (FTIR) measurements were recorded using an ATR-IR Bruker VERTEX70 instrument. The morphology, crystallinity, and size of the as-synthesized CDs were imaged using a transmission electron microscope (TEM, JEOL JEM-F200). For this, the samples were dispersed in ethanol followed by drop-casting a few drops of aliquots over the porous holey carbon-coated copper grids. pH measurements were carried out using a Metrohm 914 pH/Conductometer. The device was calibrated with three different buffers at pH levels of 4, 7 and 9.2 before we proceeded with the pH analysis of our PE-CD solution. Density functional calculations were performed without any symmetry constraint at M06-2X/def2-TZVP level.[1] Harmonic frequency calculation confirm that the ground state is a real minimum with all real values of the Hessian matrix. To understand the photoexcitation process, energy levels of the singlet and triplet excitons were calculated using time-dependent density functional method (TD-DFT) using M06-2X functional. Energies of singlet and triplet excitons are based on ground state optimized geometry. All these calculations were performed using Gaussian 16 suite of program.[2] Hirshfeld charge and charge transfer were calculated using Multiwfn program code.[3]

2) Synthesis and Characterization of PE-CDs:

a) Synthesis of PE-CDs:

1 g of polyethylene (PE) sheets were cut into smaller pieces and added to a round-bottom flask containing 60 mL of 18 M H_2SO_4. The reaction mixture was refluxed at approximately 150 °C for 3 hours, with constant stirring at 600 rpm. Over time, the transparent PE sheets gradually turned black and swelled.

Next, a $KMnO_4$ solution (1 g in 20 mL of water) was slowly added to the reaction mixture, followed by the addition of 20-25 mL of 38% H_2O_2, resulting in an orange-yellow colored solution. The solution was allowed to cool to room temperature and was then diluted with 60 mL of water. Afterward, the reaction mixture was kept at room temperature for an additional 30 minutes.

The mixture was extracted repeatedly into an organic phase using a separating funnel by adding ethyl acetate to the solution. The PE-CDs in the ethyl acetate were then filtered through Na_2SO_4 to remove any moisture. Finally, the filtered organic phase was evaporated using a rotary evaporator under reduced pressure to obtain a solid powder of PE-CDs.

b) Characterization of PE-CDs:

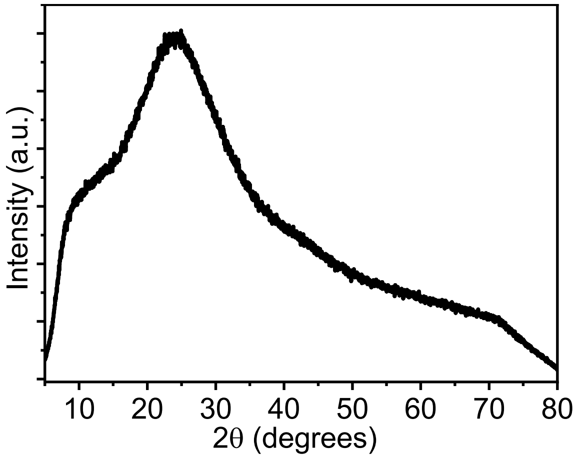

Figure S1: Powder X-ray diffraction pattern of the PE-CDs

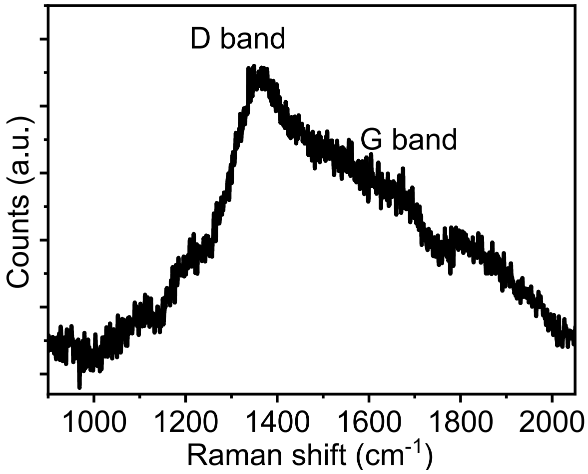

Figure S2. Raman spectrum of the PE-CDs

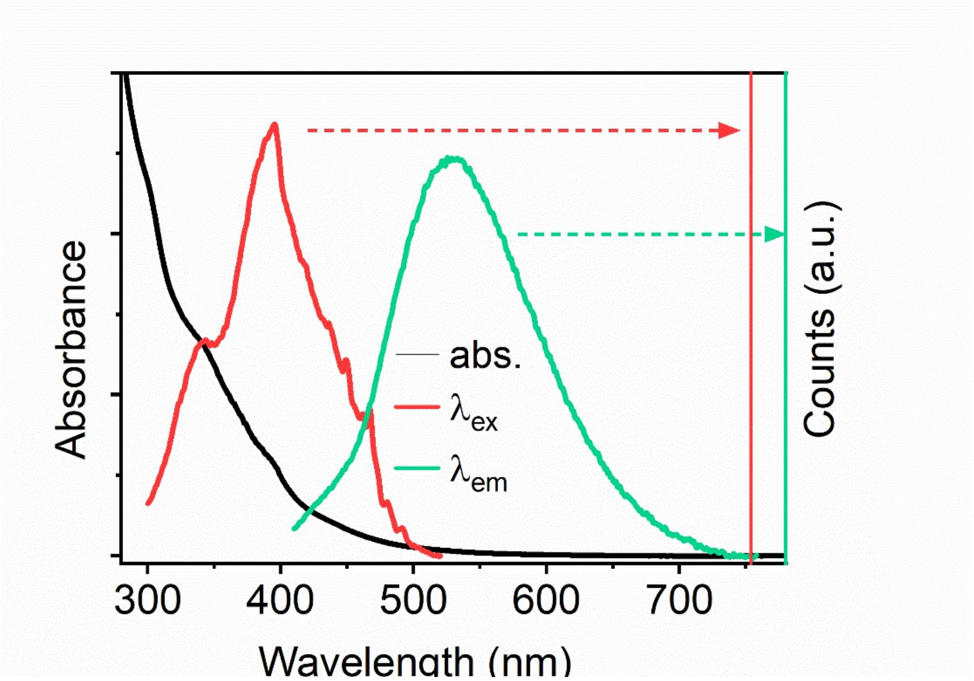

Figure S3: UV-Vis absorption, PL excitation, and PL emission spectra of a PE-CD aqueous solution

3) Autophagy Study of PE-CDs:

Supporting Note S1: We examined the self-degradation of carbon dots under light. PE-CDs self-oxidise to form CO_2 in the presence of light. PE-CDs can harvest molecular oxygen from ambient air, which plays the key role in the process. To confirm the formation of CO_2 during the degradation of PE-CDs, we prepared an aqueous solution by adding 50 mg of PE-CDs to 10 ml of water in a round-bottom flask (RB). The solution was irradiated with Xe lamp, and the lid of RB was closed with a cork. The air inside the RB was analysed with gas chromatography (GC) up to 6 hours with a regular interval of 2 hours. The GC analysis of the air inside the flask confirmed the formation of CO_2. The amount of CO_2 produced was found to increase over time, which supports the conclusion that PE-CDs self-oxidise to produce CO_2 during their degradation.

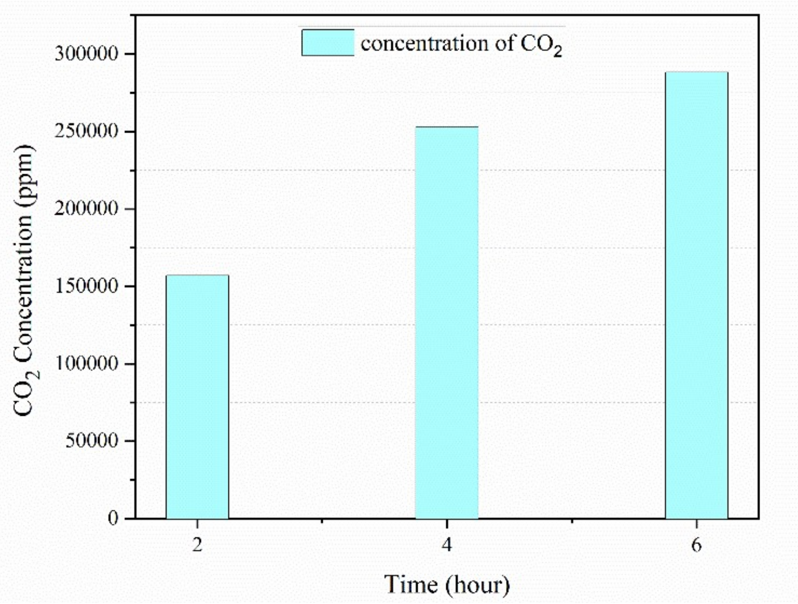

Figure S4a: Amount of CO_2 produced with different illumination times measured with GC

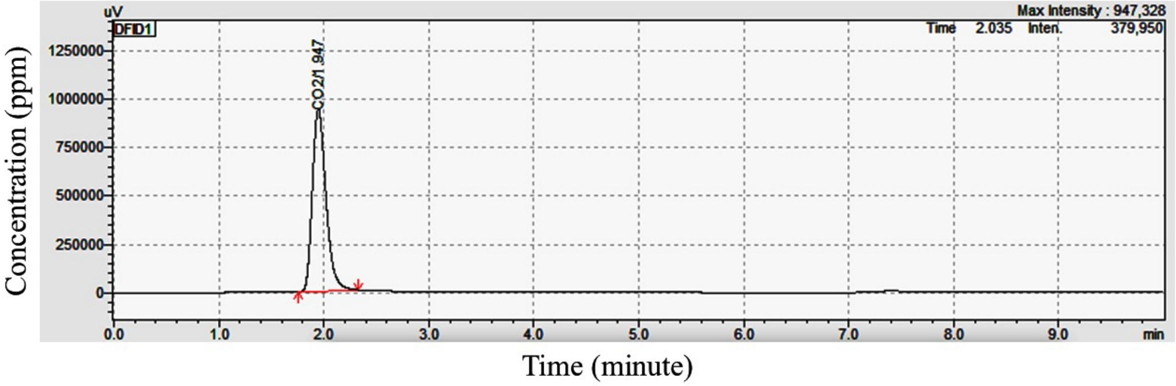

Figure S4b: CO_2 formation after 6 hours (detected by GC)

4) Oxygen harvesting property of PE-CDs

Supporting Note S2: The total O_2 (TO) content in pure water and aqueous CD solutions was quantified at room temperature using a non-invasive Ocean Optics Neofox-Kit-Probe as discussed in previous.[4-6] Briefly, a calibration curve is established across the measurement range using various N_2+O_2 gas mixtures and with a two-point standardization using ambient air (20.9% O_2) and pure N_2 (0% O_2). For the O_2 measurements, a known amount of CDs, approximately 40 mg, is added to 40 ml of milli-Q water in a round bottom flask (RB, capacity 50 ml), where the air-water interface area is ~7 cm^2, and the neck radius is ~1.5 cm. The sensing patch was affixed to the RB inner wall, ensuring it was fully submerged in the CD solutions and positioned just below the air-water interface. During the O_2 adsorption and desorption measurements, the CD solutions were stirred at 300 rpm. For the deoxygenation, N_2 gas was purged through the solution at 60-70 sccm while monitoring the O_2 desorption by noting the readings for the decrement of O_2 value at regular intervals. Once there is no further decrease in the O_2 level, the N_2 flow is halted, and the solution is left open, allowing the intake of O_2 from ambient air until saturation. Also, the O_2 values were noted at regular intervals.

First, we attempted to remove all dissolved O_2 from the CD solution by continuously purging it with N_2. We maintained this process until no further O_2 could be removed (as shown in Figure 2d in the manuscript; black line). After that, we stopped the N_2 flow, allowing O_2 to diffuse naturally into the CD solution from the air. The O_2 levels in the CD solution gradually increased, initially at a fast rate and then more slowly. We allowed this process to continue until we reached an initial saturation O_2 value (red line), noting the values at regular intervals. Figure 2d illustrates that the dotted horizontal line represents the O_2 level in pure water (approximately 310 µM). In contrast, the total O_2 (TO) content in the CD solution was found to be around 650 µM. We observed that not all O_2 molecules in the CD solution could be removed due to the strong affinity of the CDs for oxygen, resulting in a remaining O_2 (RO) value of about 110 µM. For pure water, the RO value is around 0-5 µM.

5) General Procedure for the synthesis of Quinazolin-4(*3H*)-ones:

Anthranilamide (50 mg, 0.36 mmol), Benzyl alcohol derivatives (53–60, 0.44 mmol), PE-CDs (56 mg), DMSO (2 mL) were subjected to a round bottom flask and irradiated with a full spectrum Xe light (Newport, 400 W) for 6 hours in open air at room temperature. The distance between the light source and RB was kept at 30 cm. A water-based IR filter was attached to the Xe lamp to remove the temperature effect. Besides, the temperature of the reaction mixture was constantly monitored using a thermometer to ensure no heating. After completion of the reaction, the mixture was extracted with ethyl acetate (3 ×10 mL) and washed with water (3 ×10 mL). The combined extract was dried over anhydrous Na_2SO_4. The filtrate was concentrated under reduced pressure. The product was purified by column chromatography over silica gel using *n*-hexane/ethyl acetate (3:1 v/v) as eluent to get the purified product.

6) Optimization of the reaction condition for the synthesis of Quinazolin-4(*3H*)-ones:

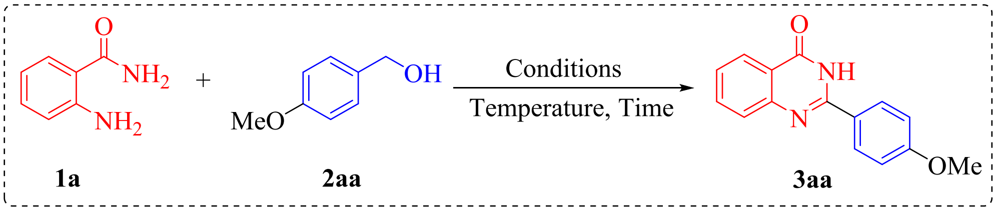

Scheme S1

Table S1: Optimization of the reaction conditions for the synthesis of quinazolin-4(*3H*)-ones

Sl No.	**Catalyst**	**Oxidant**	**Additive**	**Solvent**	**Temperature**	**Time**	**Isolated Yield**
1	-	-	-	DMSO	25 °C	24 h	-
2	-	-	KOH	DMSO	25 °C	24 h	-
3	-	H_2O_2	KOH	DMSO	25 °C	24 h	-
4	-	TEMPO	KOH	DMSO	25 °C	24 h	-
5	-	TBHP	KOH	DMSO	25 °C	24 h	-
6	-	-	-	DSMO	80 °C	24 h	-
7	-	-	KOH	DMSO	80 °C	24 h	-
8	-	H_2O_2	KOH	DMSO	80 °C	24 h	trace
9	-	TEMPO	KOH	DMSO	80 °C	24 h	trace
10	-	TBHP	KOH	DMSO	80 °C	24 h	trace
11	CDs	H_2O_2	KOH	DMSO	RT(hυ)	6 h	95%
12	CDs	-	KOH	DMSO	RT(hυ)	6 h	95%
13	CDs	-	-	DMSO	RT(hυ)	6 h	95%
14	CDs	-	-	-	RT(hυ)	6 h	40%
15	CDs	-	-	DMSO	80 °C	5 h	80%
16	-	-	-	DMSO	RT(hυ)	6 h	-
17	(O_2 environment)	-	-	DMSO	RT(hυ)	8 h	-
18	CDs	-	Hydroquinone	DMSO	RT(hυ)	6 h	30%

Reaction Conditions: 1a (50 mg, 0.36 mmol), 2aa (126 mg, 0.91 mmol), CD (51 mg), oxidant (0.36 mmol), Additive (0.36 mmol), solvent (2 ml) at different conditions. hυ is 400 W of entire Xe light source

[b] Isolated yield of pure product.

Supporting Note S3: The investigations were carried out using KOH and DMSO in neat conditions (**Table S1, entry 2**). KOH and DMSO together form a suspension that was assumed to meet the prerequisite conditions for the solubility of Schiff bases. One of the intermediate steps of the reaction is Schiff base formation. However, no yield of the desired product was observed till 24 hours at room temperature. The reaction in the absence of KOH did not result in the formation of products (**Table S1, entry 1**). For the oxidative formation of quinazolin-4(*3H*)-ones, the alcohol must first be oxidized to its corresponding aldehyde. Then, the anthranilamide reacts with the in-situ generated aldehyde to generate the Schiff base, followed by cyclization and dehydrogenation to yield the product.[14] Hence, a few oxidizing agents were tested with KOH and DMSO at room temperature to trigger the reaction, but no characteristic yield of the corresponding product was seen (**Table S1, entries 3-5**). The reactions were further tested at a higher temperature of 80 °C (**Table S1, entries 6-10**) to see the activity of the oxidants, but only a trace amount of products were formed. Because of the requirement for higher activation energy, the reaction becomes too slow with the oxidants alone.[15] Hence, there is a requirement for a catalyst to lower the activation energy so that the reaction proceeds faster. In this regard, we used PE-CDs as photocatalysts for the reaction with an oxidant (**Table S1, entry 11**) and illuminated the reaction using a 400 W Xe arc lamp. The reaction yielded 95% of the corresponding product after 6 hours, demonstrating the catalytic efficiency of the PE-CDs. Next, a reaction was tested in the absence of the oxidants to check the efficiency of the oxygen harvesting PE-CDs as oxidant cum catalyst (**Table S1, entry 12**). It resulted in the formation of the same amount of products, confirming the superiority of PE-CDs as an oxidant cum catalyst. A reaction without KOH found the same amount of product formation, i.e., 95% (**Table S1, entry 13**). The reaction performed in the absence of DMSO reduced the yield to 40% (**Table S1, entry 14**). On reducing the time to 5 hours, the yield was reduced to 80% (**Table S1, entry 15**). After the optimization of the reaction temperature, it was seen that the formation of the corresponding quinazolin-4(*3H*)-ones were optimum on applying a full spectrum of 400 W of Xe arc lamp for 6 hours in PE-CD as a photocatalyst, molecular O_2 air as oxidant and DMSO as a solvent. A solvent optimization study was conducted while keeping the other parameters constant, and DMSO was found to be the best solvent for the transformation due to the enhanced solubility of the intermediate formed during the process in DMSO. A reaction performed in the absence of PE-CDs (**Table S1, entry 16**) resulted in no product formation, confirming the requirement of CDs as oxidant cum catalyst for the transformation. A controlled reaction was done in the O_2 environment in the absence of PE-CDs to demonstrate its role in the oxidative synthesis of quinazolin-4(*3H*)-ones (**Table S1, entry 17**). From the result, it was concluded that the molecular O_2 is insufficient to lower the reaction's activation energy for oxidative transformation without CDs. The reaction is assumed to proceed through the oxidation of the benzyl alcohol to benzaldehyde through a radical process followed by Schiff base formation, cyclization, and dehydrogenation. To confirm the radical oxidation process, a radical scavenger was used along with the optimized condition (**Table S1, entry 18**); and a lower yield of 30% confirmed our hypothesis.

7) EPR Spectrum of Singlet Oxygen Quenched During the Reaction

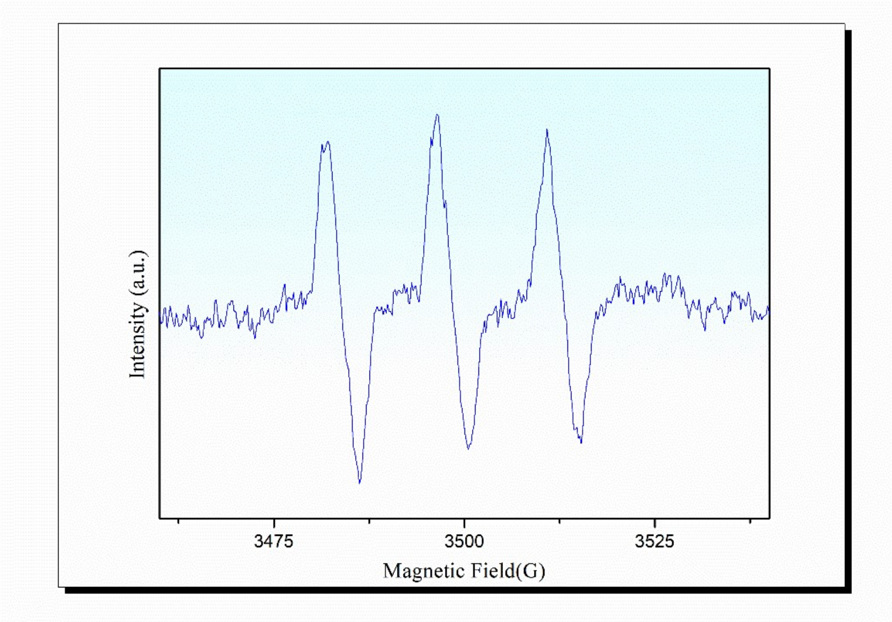

Figure S5: EPR detection of singlet oxygen trapped by TEMP (2,2,6,6-tetramethylpiperidine)

8) Mass Spectrum of TEMPO-Adduct

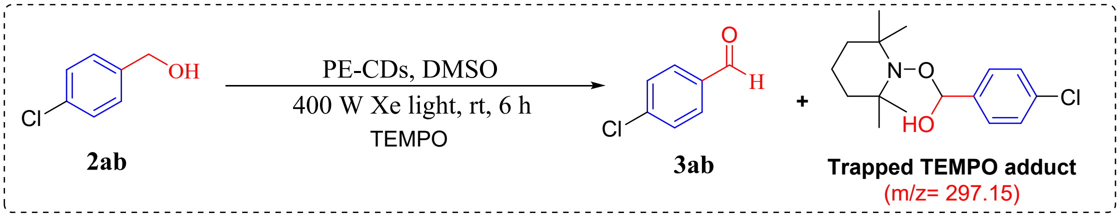

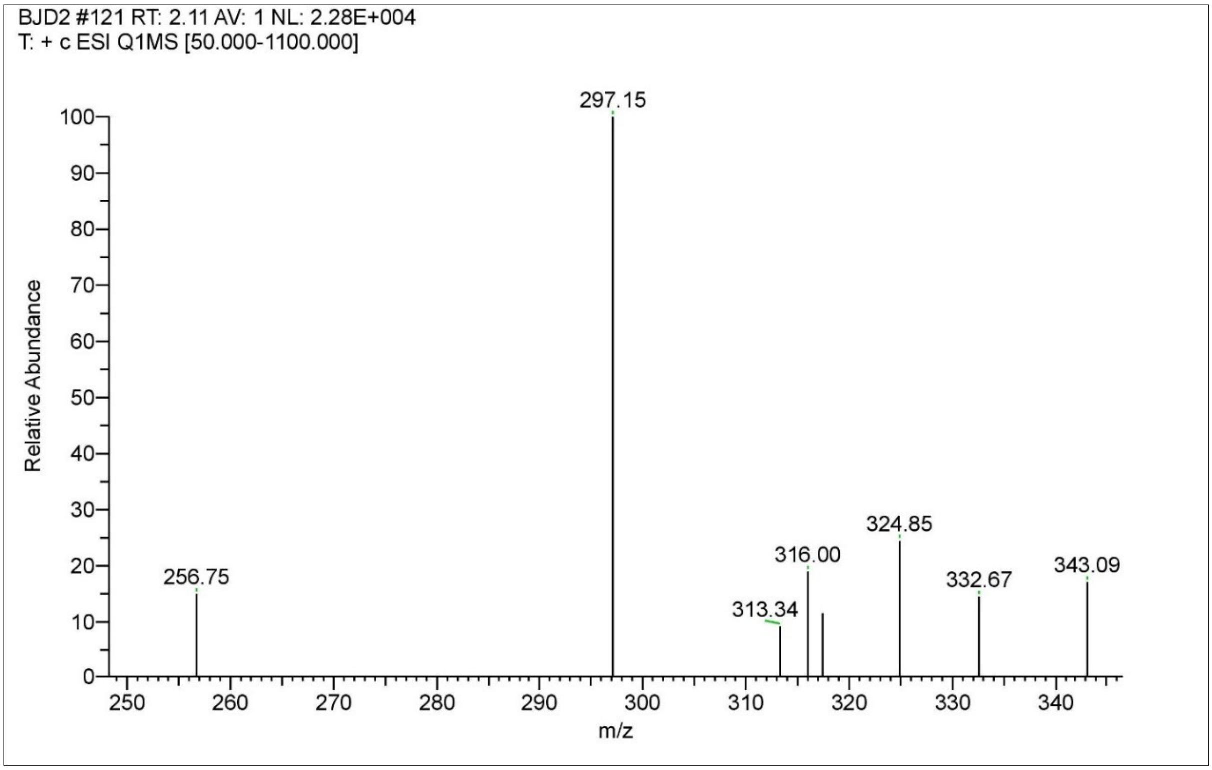

Figure S6: Mass spectrum of TEMPO adduct

9) In-situ spectroscopic detection of ROS:

Supporting Note S4:

Tracking of singlet oxygen ($^1O_2$) :

The generation of $^1O_2$ has been investigated using 9,10-diphenylanthracene (DPA). A solution of 30 ml containing 60 µM DPA in ethanol was mixed with 10 ml of an ethanolic carbon dot solution that contains 0.35 mg of PE-CDs. DPA exhibits characteristic absorption peaks around 355-375 nm. When DPA reacts with $^1O_2$, it forms a thermostable endoperoxide, which does not absorb light at the same wavelengths as DPA.

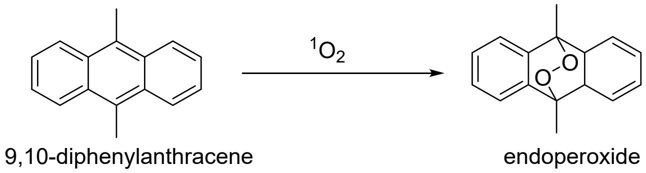

Scheme S2: Reaction of $^1O_2$ with DPA

Therefore, by monitoring the decrease in the UV absorption peak within this wavelength range, the reaction between DPA and $^1O_2$ has been tracked and the generation of $^1O_2$ by PE-CDs has been detected and quantified. Gradual increase in the concentration of $^1O_2$ over time confirms the excellent ability of PE-CDs to produce $^1O_2$. The generation of $^1O_2$ was continuously monitored up to 120 minute

Tracking of superoxide radical (O_2^{-}•):

The generation of superoxide has been investigated using Nitro blue triazolium chloride (NBT). An aqueous solution of 30 ml containing 12.5 μM NBT was mixed with 10 ml aquous PE-CD solution that contains 0.35 mg of PE-CDs. NBT exhibits characteristic absorption peaks at 259 nm. When it reacts with O_2^{-}•, it forms formazan, which does not absorb light at the same wavelengths as NBT.

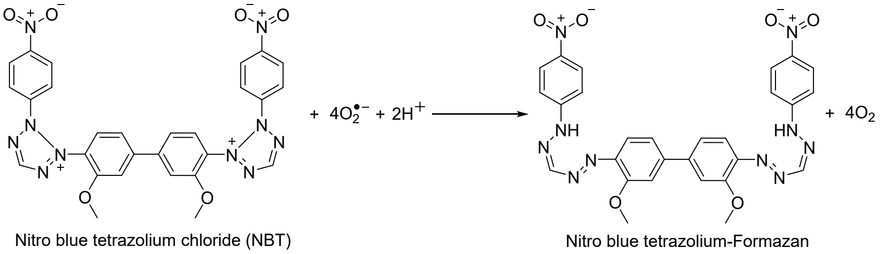

Scheme S3: Reaction of O_2^{-}• with NBT

Therefore, by monitoring the decrease in the UV absorption peak within this wavelength, the reaction between NBT and O_2^{-}• has been tracked and the generation of O_2^{-}• by PE-CDs has been detected and quantified. A gradual increase in the concentration of O_2^{-}• over time confirms the excellent ability of PE-CDs to produce O_2^{-}•. The generation of O_2^{-}• was continuously monitored up to 120 minutes and the concentration was observed to be 671 μmol/g after 120 minutes.

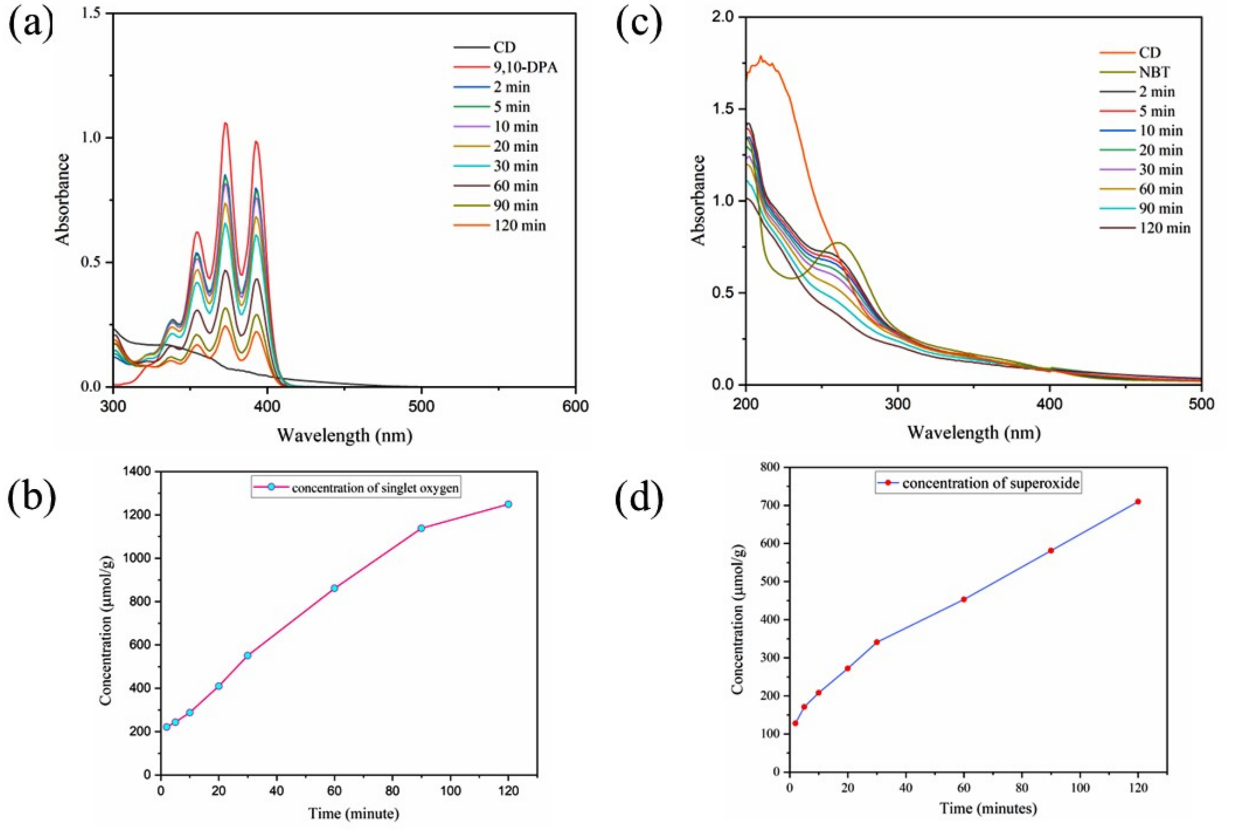

Figure S7: (a) Time-dependent UV–Vis spectra of DPA solution (60 μM) containing PE-CDs (0.35 mg). (b) Concentration of singlet oxygen generated in μmol/g at various time intervals by PE-CDs (0.35 mg) (c) Time-dependent UV–Vis spectra of NBT solution (12.5 μM) containing PE-CDs (0.35 mg). (d) Concentration of singlet oxygen generated in μmol/g at various time intervals by PE-CDs (0.35 mg). All are Xe-lamp illumination in ambient conditions.

10) Computational Study of Mechanism:

Supporting Note S5: A schematic Jablonski diagram showing the singlet and triplet (S_1 and T_1) excitons based on ground state singlet (S_0) is presented in Fig S8a. The intersystem crossing energy gap (ΔE_{ISC}) was calculated based on the energy difference between the singlet and triplet excitons ($\Delta E_{ISC} = E_{S1}-E_{T1}$). According to Arrhenius equation ($k\text{isc} \propto \exp(-\Delta E_{ISC}/kT)$), the rate of ISC energy transfer reaches its maximum when the ISC energy gap (ΔE_{ISC}) becomes close to zero. It is evident from Scheme 3 that ΔE_{ISC} is very small indicating significant rate of ISC. Thus, ISC is quite a feasible process with subsequent triplet-triplet energy transfer from T_1 to $^3O_2$ *via* a Dexter multi-electron transfer process.[7,8]

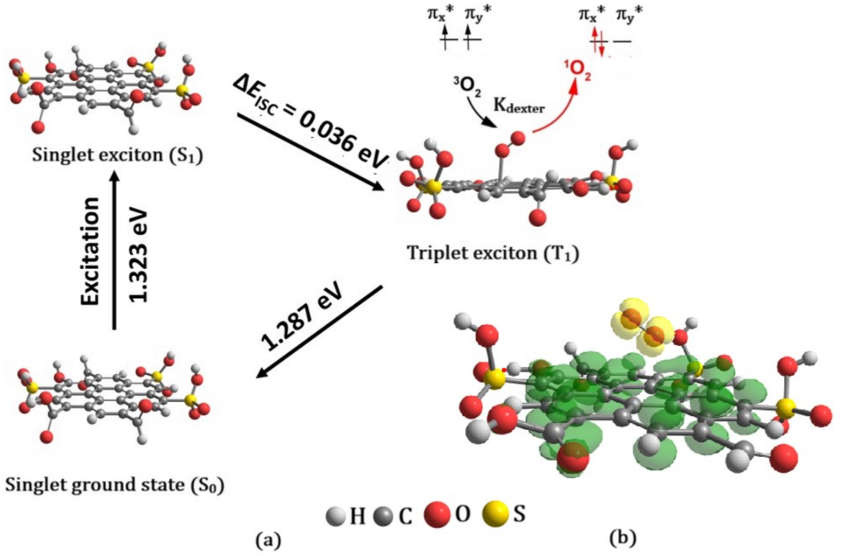

Figure S8: (a) Schematic Jablonski diagram showing ground state singlet (S_0), singlet and triplet exciton (S_1 and T_1) and energy gap for intersystem crossing (ΔE_{ISC}) and (b) charge transfer from PE-CDs to dioxygen. Yellow colour represents charge accumulation and green colour represents charge depletion.

Figure S8b shows charge (Hirshfeld) transfer from PE-CDs to the π_x^* and π_y^* antibonding orbital of dioxygen resulting in the spin-flip and elongation of the O-O bond length from 1.188 Å for the ground state of dioxygen to 2.214 Å in the dioxygen adsorbed on PE-CDs.[9]

Figure S9 shows reaction mechanism (top) along with the energetics (ΔG, kcal/mol) and optimized geometries (bottom). Reaction of 2 and 3 produces intermediate 4 and the process is found to be exergonic by 4.2 kcal/mol. Intermediate 4 then gets converted to 5 through a transition state ($TS_{4\text{-}5}$) which involves hydrogen atom transfer from NH_2 to the oxygen atom of CO. The calculated barrier for the process is 1.9 kcal/mol. In $TS_{4\text{-}5}$, the N$\cdots$H and O$\cdots$H distances are 1.550 and 2.253 Å respectively. Intermediate 5 then gets converted to the final product 6 through another transition state ($TS_{5\text{-}6}$) and the barrier for the process is 3.0 kcal/mol. In $TS_{5\text{-}6}$, C-N bond formation takes place to form a six membered ring in 6. Thus, owing to the favourable energetics of the reactions, the plausible mechanism is quite likely.

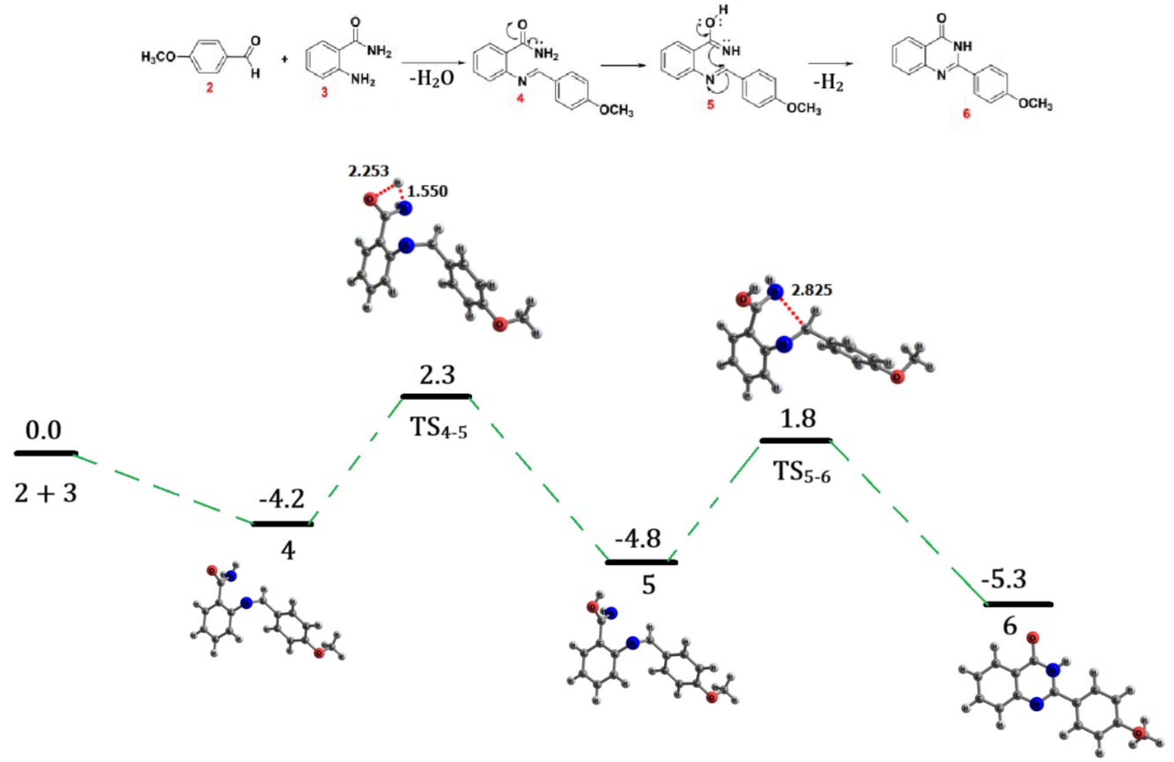

Figure S9. Plausible mechanism and energetics for the formation of 6 from 2 and 3. Relative energies (Δ*G*) are in kcal/mol. Bond lengths are in Å.

11) Calculation of Eco-Scale

Supporting Note S6: An important factor in green chemistry is the Eco Scale. Eco Scale of the synthetic procedures to achieve the products of table 4 has been calculated[10] and based on this analysis, the environmental friendliness of the methodology has been determined. An Eco Scale of above 75 is considered an excellent green method, above 50 is acceptable, while scores below 50 indicate inadequate eco-friendliness. Therefore, we term our methodology as a green method.

Eco Scale can be calculated as:

Eco Scale = 100 - sum of the individual penalties

The individual penalties for the Scheme 1 have been calculated as follows:

Table S1: Penalty points to calculate Eco Scale for entry 3aa, Table 2

Sl No.	Parameters	Values	Penalty Points

1	Yield	(100-95)/2	2.5
2	Price of the Substrates	< $ 10	0
3	Safety[a]	Not dangerous	0
4	Technical setup	Photochemical Apparatus	2
5	Temperature/Time	Room Temperature	0
6	Workup and purification	Removal of solvent with bp < 150 °C	0
		Total penalty points	4.5

[a] Based on the hazard warning symbols

Hence, Eco Scale = 100-4.5=95.5

The calculated Eco Scale for the other entries is as follows:

Entries from Table 4	**Eco-Scale**	**Entries from Table 4**	**Eco-Scale**
3ab	92	3ah	93
3ac	91	3ai	84.5
3ad	95.5	3aj	86
3ae	93	3ak	83
3af	95.5	3al	87
3ag	89		

12) Spectral Data of Representative Products

2-(4-methoxyphenyl)quinazolin-4(*3H*)-one (Table 1, 3aa)

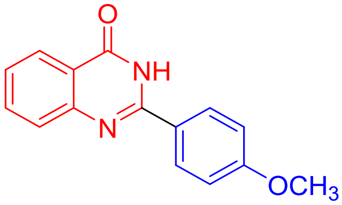

(Off White Solid, mp: 246-248 °C). ^{1}H NMR (400 MHz, $CDCl_3$) δ 10.66 (s, 1H), 8.30 (d, J = 8.1 Hz, 1H), 8.13 (d, J = 8.8 Hz, 2H), 7.85 (dd, J = 3.7, 1.9 Hz, 2H), 7.48 (m, 1H), 7.07 (d, J = 8.9 Hz, 2H), 3.91 (s, 3H).MS (ESI) m/z: [M+H]+ calcd for $C_{15}H_{12}N_2O_2H$ 253.08; Found 253.09.

2-(p-tolyl)quinazolin-4(*3H*)-one (Table 1, 3ad)

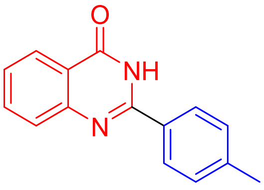

(Off White Solid, mp: 240-241 °C).^{1}H NMR (500 MHz, $CDCl_3$) δ 11.55 (s, 1H), 8.33 (d, J = 7.9 Hz, 1H), 8.15 (d, J = 7.8 Hz, 2H), 7.89 – 7.77 (m, 2H), 7.50 (t, J = 7.4 Hz, 1H), 7.39 (d, J = 7.8 Hz, 2H), 2.47 (s, 3H).MS (ESI) m/z: $[M+H]^+$ calcd for $C_{15}H_{12}N_2O$ 237.09; Found 237.06

2-(m-tolyl)quinazolin-4(*3H*)-one (Table 1, 3af)

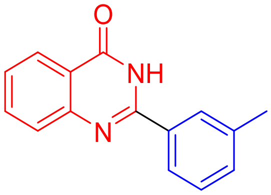

(Off White Solid, mp: 221- 223 °C). ^{1}H NMR (400 MHz, $CDCl_3$) δ 10.71 (s, 1H), 8.33 (d, J = 7.8 Hz, 1H), 8.01 (s, 1H), 7.93 (d, J = 7.8 Hz, 1H), 7.83 (t, J = 9.0 Hz, 2H), 7.53 – 7.39 (m, 3H), 2.51 (s, 3H). MS (ESI) m/z: $[M+H]^+$ calcd for $C_{15}H_{12}N_2O$ 237.09; Found 237.07

2-(3-bromophenyl)quinazolin-4(*3H*)-one(Table 1, 3ag)

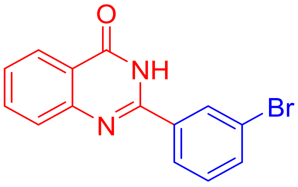

(Off White Solid, mp: 289- 290 °C). ^{1}H NMR (400 MHz, DMSO) δ 12.69 (s, 1H), 8.45 (t, J = 1.8 Hz, 1H), 8.24 (m, 2H), 7.92 (m, 1H), 7.89 – 7.80 (m, 2H), 7.66 – 7.57 (m, 2H). MS (ESI) m/z: $[M+H]^+$ calcd for $C_{14}H_9BrN_2O$ 300.98; Found 301.00

2-(4-fluorophenyl)quinazolin-4(*3H*)-one (Table 1, 3ah)

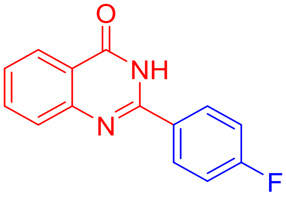

(Off White Solid, mp: 284- 287 °C). ^{1}H NMR (400 MHz, DMSO) δ 12.57 (s, 1H), 8.29 – 8.22 (m, 2H), 8.15 (dd, J = 8.0, 1.6 Hz, 1H), 7.84 (m, 1H), 7.74 (d, J = 8.2 Hz, 1H), 7.57 – 7.49 (m, 1H), 7.45 – 7.36 (m, 2H).^{13}C NMR (100 MHz, DMSO) δ 163.22 (d, J = 12.3 Hz), 162.68, 151.86, 149.13, 135.13, 130.85 (d, J = 8.9 Hz), 129.71 (d, J = 2.7 Hz), 127.94, 127.10, 126.33, 121.36, 116.11 (d, J = 21.9 Hz).MS (ESI) m/z: [M+H]+ calcd for $C_{14}H_9FN_2O$ 241.06; Found 241.06.

2-(2-bromophenyl)quinazolin-4(*3H*)-one (Table 1, 3ai)

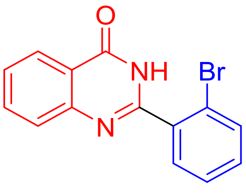

(Off White Solid, mp: 297-299 °C). ^{1}H NMR (400 MHz, CDCl$_3$) δ 11.10 (s, 1H), 8.24 (d, J = 7.9 Hz, 1H), 7.85 – 7.77 (m, 2H), 7.70 (m, 2H), 7.49 (m, 2H), 7.42 – 7.35 (m, 1H). ^{13}C NMR (100 MHz, CDCl$_3$) δ 162.84, 152.22, 148.97, 134.95, 133.72, 131.97, 131.22, 127.98, 127.89, 127.38, 126.50, 125.05, 121.13, 121.01. MS (ESI) m/z: [M+H]$^+$ calcd for $C_{14}H_9BrN_2O$ 300.98; Found 300.99

13) ^{1}H and ^{13}C Spectra of Representative Products

^{1}H spectrum of 2-(4-methoxyphenyl)quinazolin-4(*3H*)-one (3aa)

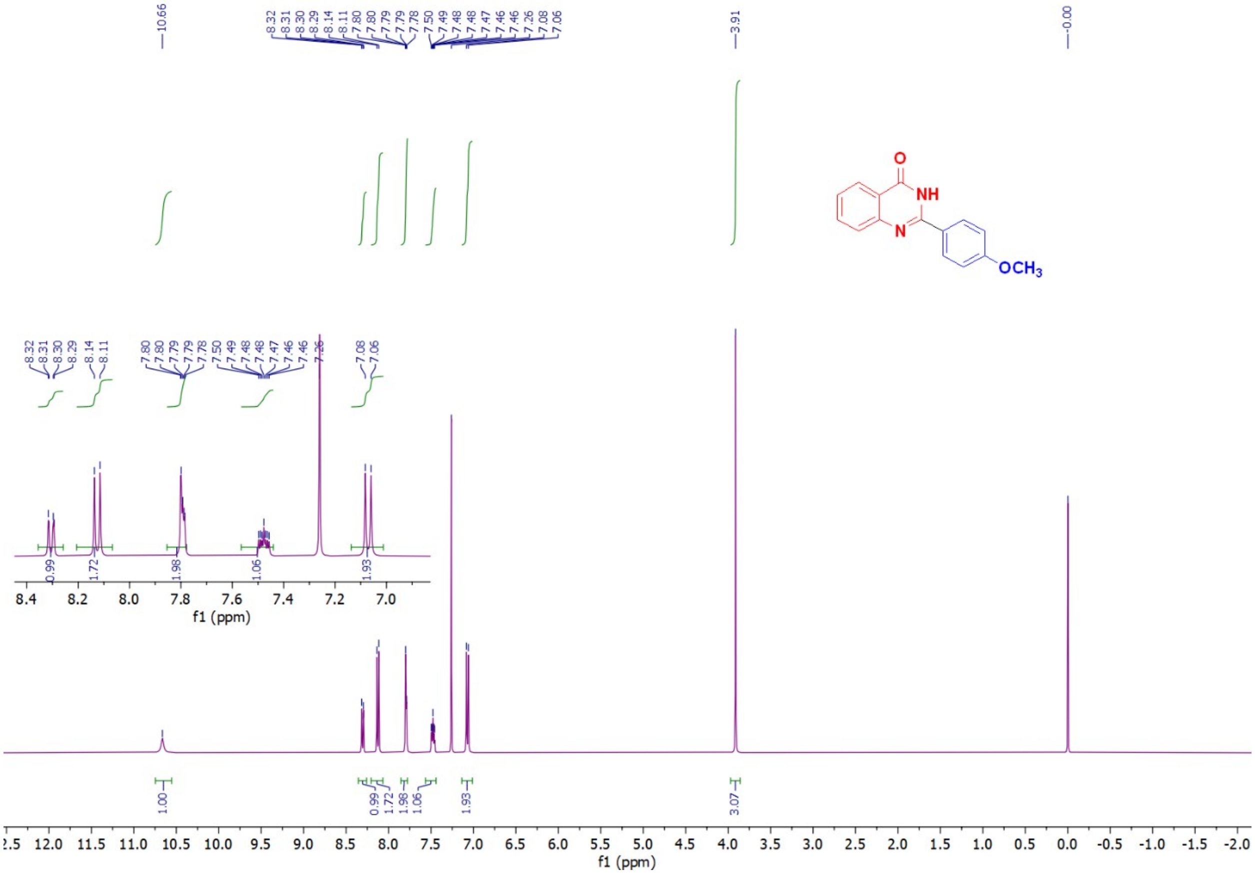

^{1}H spectrum of 2-(p-tolyl)quinazolin-4(*3H*)-one (3ad)

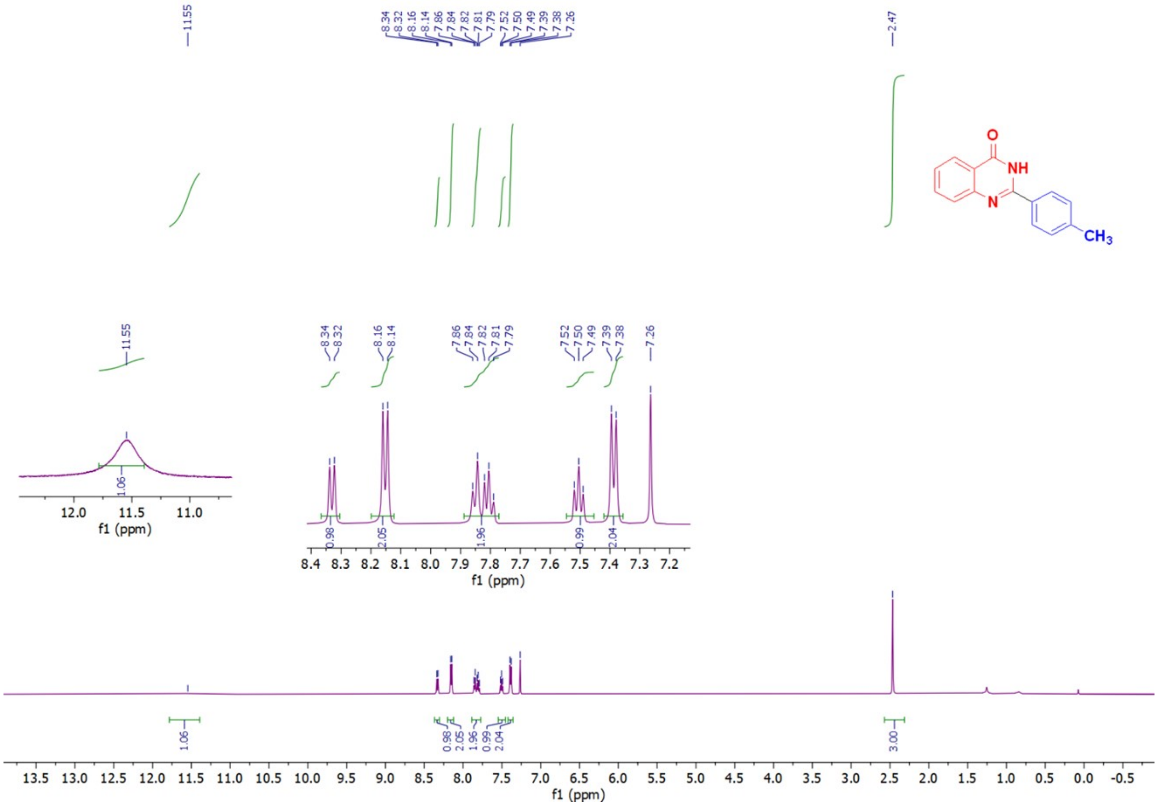

^{1}H spectrum of 2-(m-tolyl)quinazolin-4(*3H*)-one (3af)

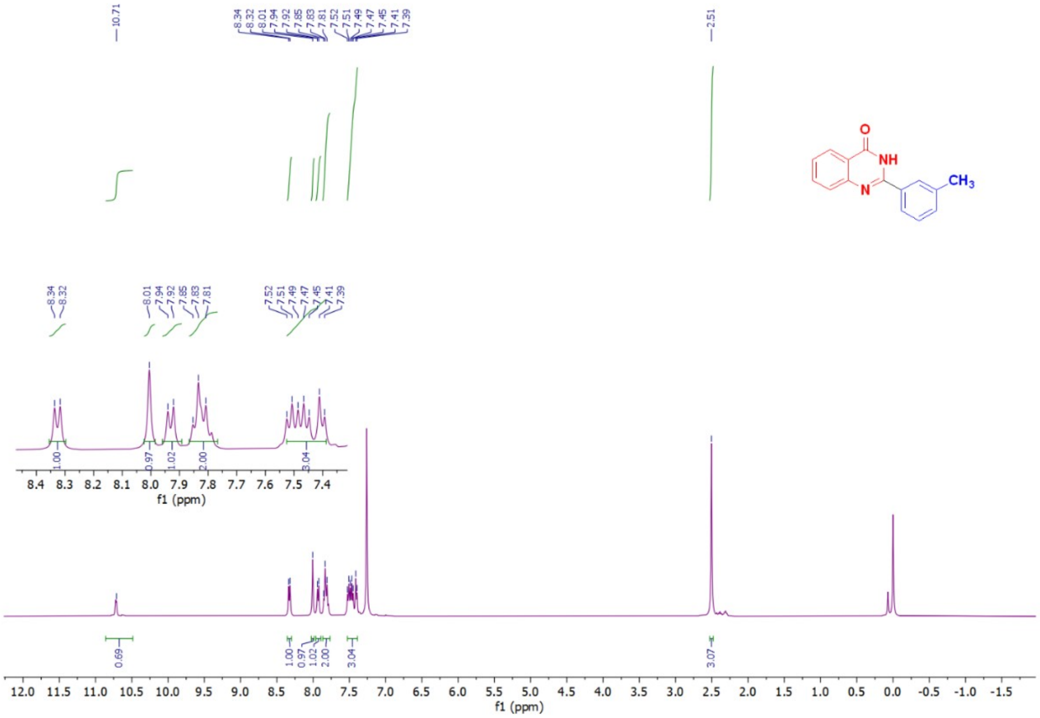

^{1}H spectrum of 2-(3-bromophenyl)quinazolin-4(*3H*)-one (Table 1, 3ag)

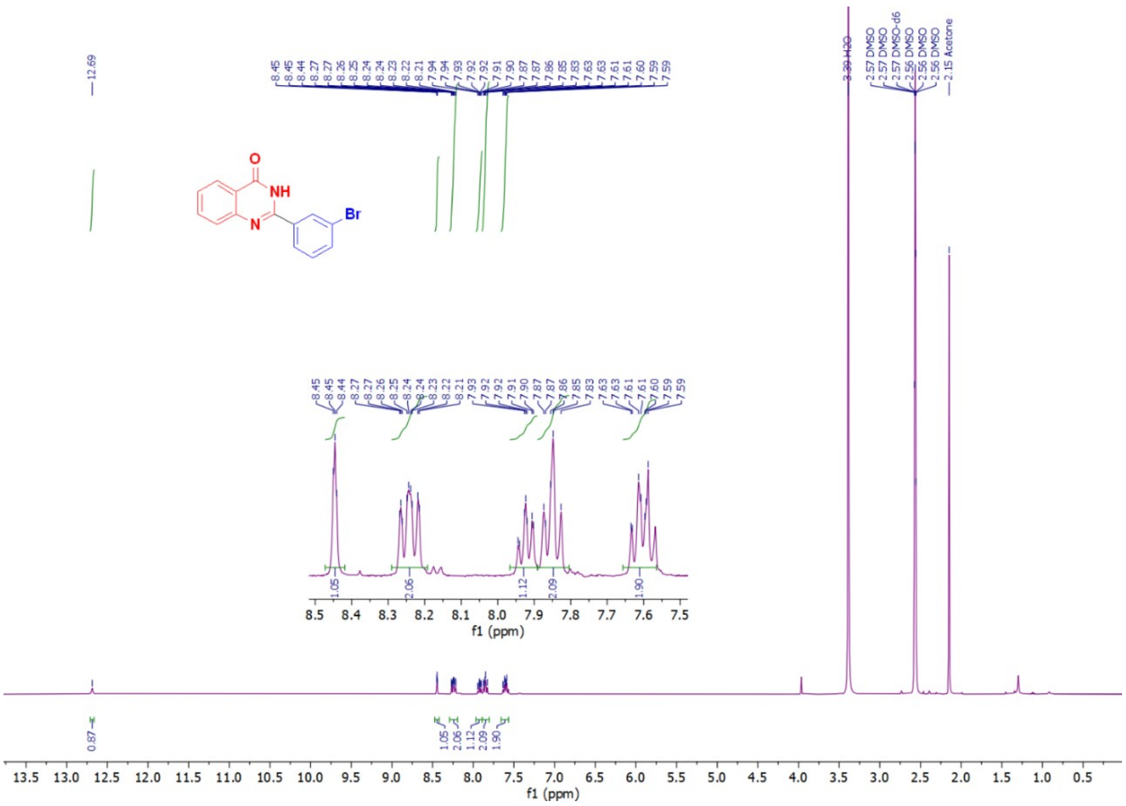

^{1}H spectrum of 2-(4-fluorophenyl)quinazolin-4(*3H*)-one (Table 1, 3ah)

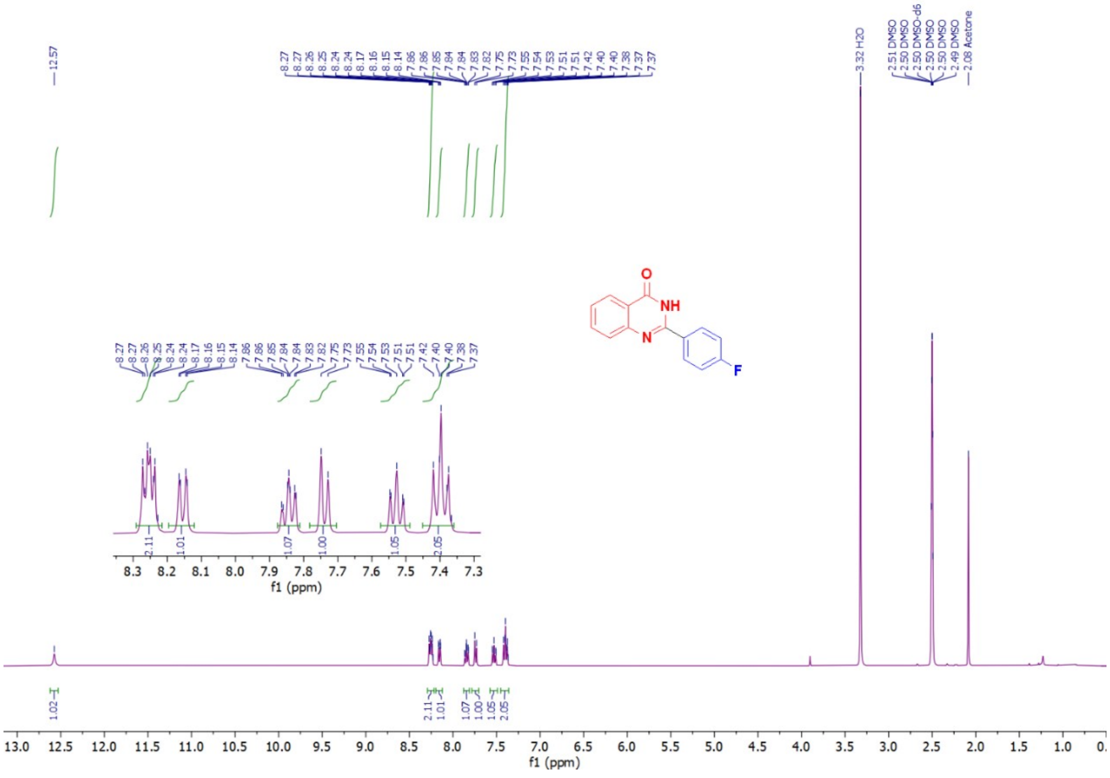

^{13}C spectrum of 2-(4-fluorophenyl)quinazolin-4(*3H*)-one (Table 1, 3ah)

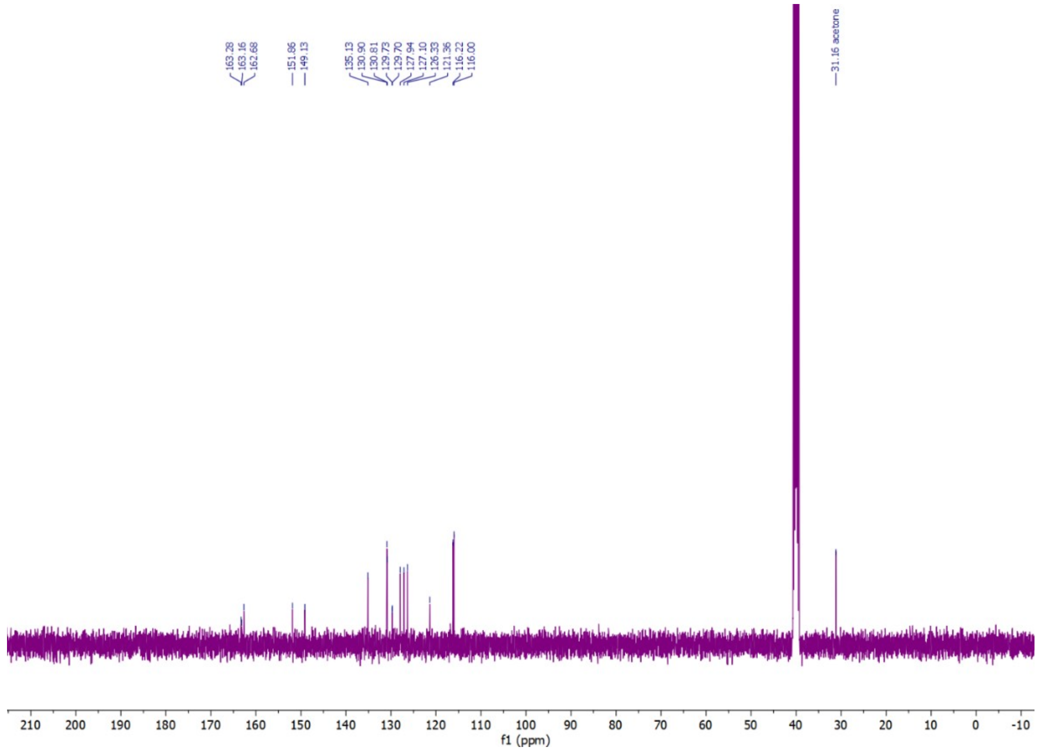

^{1}H spectrum of 2-(2-bromophenyl)quinazolin-4(*3H*)-one (Table 1, 3ai)

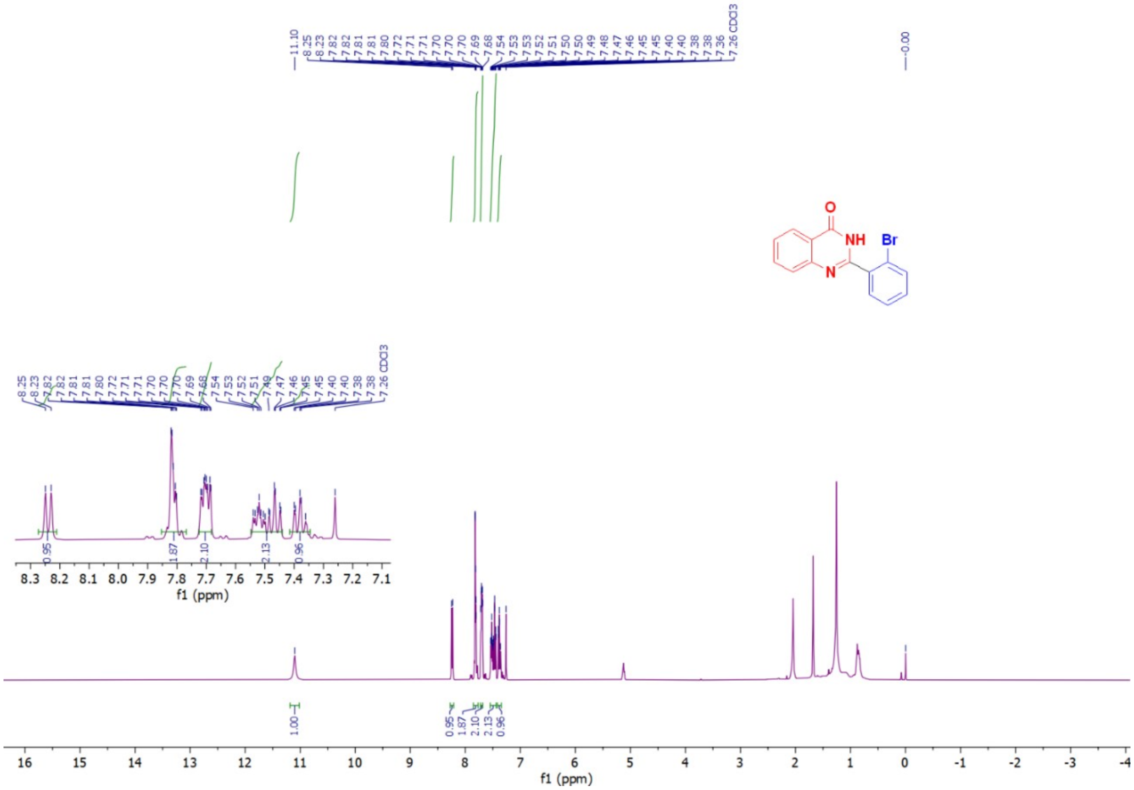

^{13}C spectrum of 2-(2-bromophenyl)quinazolin-4(*3H*)-one (Table 1, 3ai)

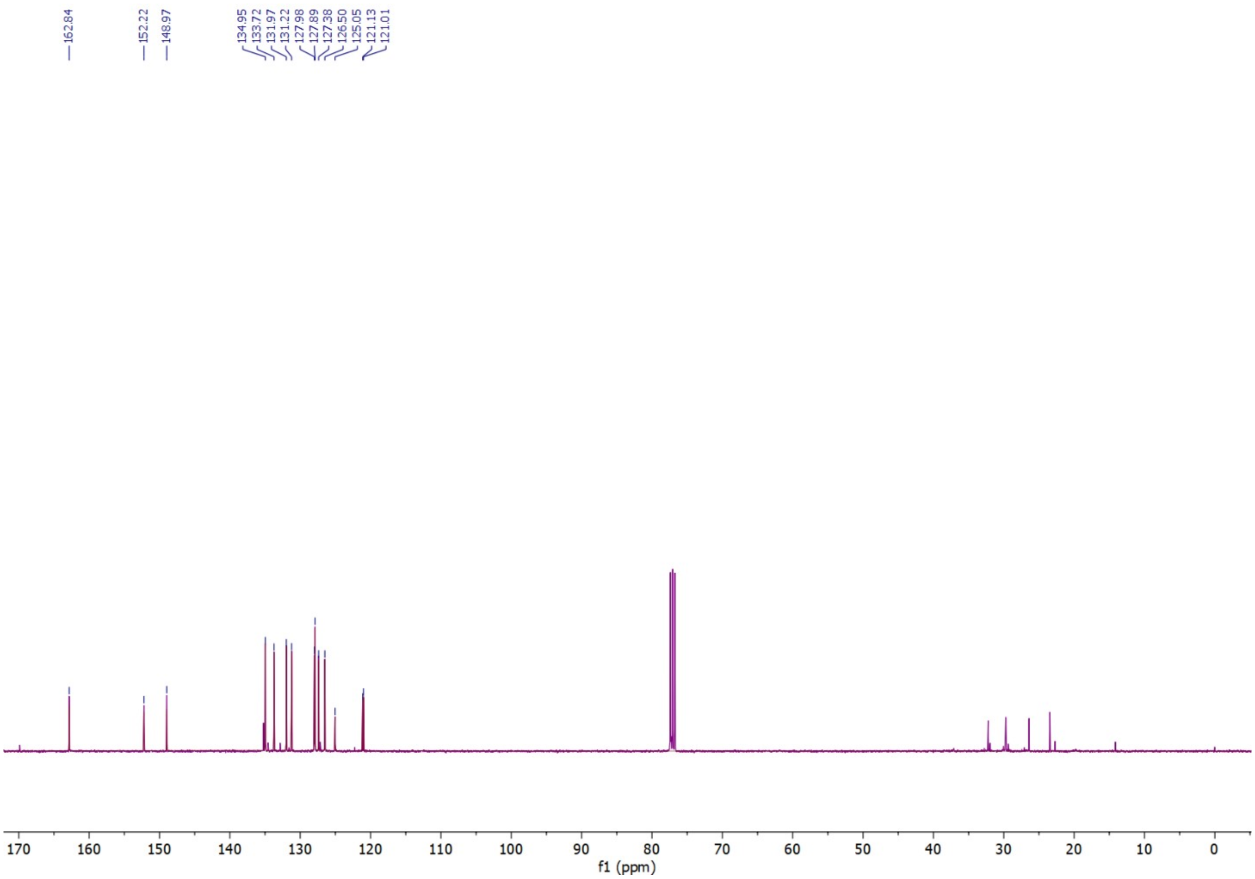

14) References

1) Y. Zhao, D. G. Truhlar, *Theor. Chem. Acc.*, 2008, **120**, 215-241.

2) M. J. Frisch, G. W. Trucks, H. B. Schlegel, G. E. Scuseria, M. A. Robb, J. R. Cheeseman, G. Scalmani, V. Barone, G. A. Petersson, H. Nakatsuji, X. Li, M. Caricato, A. V. Marenich, J. Bloino, B. G. Janesko, R. Gomperts, B. Mennucci, H. P. Hratchian, J. V. Ortiz, A. F. Izmaylov, J. L. Sonnenberg, D. Williams-Young, F. Ding, F. Lipparini, F. Egidi, J. Goings, B. Peng, A. Petrone, T. Henderson, D. Ranasinghe, V. G. Zakrzewski, J. Gao, N. Rega, G. Zheng, W. Liang, M. Hada, M. Ehara, K. Toyota, R. Fukuda, J. Hasegawa, M. Ishida, T. Nakajima, Y. Honda, O. Kitao, H. Nakai, T. Vreven, K. Throssell, J. A. Montgomery, Jr., J. E. Peralta, F. Ogliaro, M. J. Bearpark, J. J. Heyd, E. N. Brothers, K. N. Kudin, V. N. Staroverov, T. A. Keith, R. Kobayashi, J. Normand, K. Raghavachari, A. P. Rendell, J. C. Burant, S. S. Iyengar, J. Tomasi, M. Cossi, J. M. Millam, M. Klene, C. Adamo, R. Cammi,

J. W. Ochterski, R. L. Martin, K. Morokuma, O. Farkas, J. B. Foresman and D. J. Fox, Gaussian 16, revision A.03; Gaussian, Inc.: Wallingford, CT, (2016).

3) T. Lu and F. Chen, Multiwfn. *J. Comput. Chem.* 2012, **33**, 580.

4) S. Mondal, P. E. Karthik, L. Sahoo, K. Chatterjee, M. Satish, U. K. Gautam, *Nanoscale* 2020, **12**, 10480

5) S. Mondal, S. R. Das, L. Sahoo, S. Dutta, U. K. Gautam, *J. Am. Chem. Soc*., 2022, **144**, 2580–2589.

6) M. W. Kanan, D. G. Nocera, *Science* 2008, **321**, 1072.

7) M. Tamtaji, A. Tyagi, C. Y. You, P. R. Galligan, H. Liu, Z. Liu, R. Karimi, Y. Cai, A. P. Roxas, H. Wong, Z. Luo, *ACS Appl. Nano Mater.*, 2021, **4**, 7563–7583.

8) M. Tabachnyk, B. Ehrler, S. G´elinas, M. L. Böhm, B. J. Walker, K. P. Musselman, N. C. Greenham, R. H. Friend and A. Rao, *Nat. Mater.*, 2014, **13**, 1033–1038.

9) G. Yang, J. Zhu, P. Yuan, Y. Hu, G. Qu, B. A. Lu, X. Xue, H. Yin, W. Cheng, J. Cheng, W. Xu, J. Li, J. Hu, S. Mu, J. N. Zhang, *Nat. Commun.*, 2021, **12**, 4–13.

10) K.V. Aken, L. Strekowski, L. Patiny, *Beilstein J. Org. Chem*., 2006, **2**, 3.